厚生労働科学研究費補助金

新型インフルエンザ等新興・再興感染症研究事業

2012年に発生した新型ヒトコロナウイルス侵入に備えた診断、治療法確立のための動物モデル開発とSARS-CoVとの鑑別に関する研究

平成26年度　総括研究報告書

研究代表者　岩田　奈織子

平成27　(2015) 年　3月

厚生労働科学研究費補助金
平成26年度　新型インフルエンザ等新興・再興感染症研究推進事業

2012年に発生した新型ヒトコロナウイルス侵入に備えた診断、治療法確立のための動物モデル開発とSARS-CoVとの鑑別に関する研究

研究代表者：　岩田　奈織子（国立感染症研究所感染病理部）

協力研究者：　岡村　匡史（国立国際医療研究センター研究所感染症制御研究部）
永田　典代（国立感染症研究所感染病理部）
鈴木　忠樹（国立感染症研究所感染病理部）
中島　典子（国立感染症研究所感染病理部）
佐藤　由子（国立感染症研究所感染病理部）
福士　秀悦（国立感染症研究所ウイルス第一部）
松山　州徳（国立感染症研究所ウイル第三部）
梁　明秀（横浜市立大学医学部）

目次

Ⅰ.　総括研究報告

厚生労働科学研究費補助金（新型インフルエンザ等新興・再興感染症研究事業）
総括研究報告書

「2012年に発生した新型ヒトコロナウイルス侵入に備えた診断、治療法確立のための動物モデル開発とSARS-CoVとの鑑別に関する研究」

研究代表者　岩田　奈織子　国立感染症研究所　主任研究官

研究要旨： 2012年9月に中東で重症呼吸器疾患を起こす患者が報告された。2003年に大流行した重症急性呼吸器症候群(SARS)の再興かと疑われたが、患者からは新規のヒトコロナウイルスである中東呼吸器症候群コロナウイルス(MERS-CoV)が分離された。現在も流行は中東中心だが、欧州地域では輸出症例も頻発している。そのため、日本でも今後、国内侵入を想定した対応が必要で、病原性の解明、診断、治療、予防、防疫対策が急務である。また類似の症状を示すSARSとの鑑別診断も公衆衛生学上、重要である。そこで、本研究ではMERS-CoVに対し病原性の解明、ワクチンなどの有効性試験、ウイルス増殖部位の同定および免疫応答を詳細に検討するため感染動物モデルの確立とSARS-CoVと鑑別可能な病理診断系の確立を行う。昨年度はマウスおよびラットのMERS-CoVに対する感受性を検討し、これらの動物には感染が成立しない事を明らかにした。この結果から小動物感染モデルを確立するには、MERS-CoVのレセプターであるヒトCD26発現遺伝子改変マウスの作製が必要となった。そこで、本年度はヒトCD26発現遺伝子改変マウスの作製を行った。10匹のファウンダーマウスが獲得でき、現在、これらの系統を確立中である。系統化されたマウスのMERS-CoV感受性を調べ、系統を選択していく予定である。さらに、ヒトCD26発現遺伝子改変マウスの第二世代として、ノックインマウス作製を計画しており、本年度はマウスにノックインするヒトCD26遺伝子について、MERS-CoVの感染性が得られる領域を調べるため、マウスCD26とヒトCD26のキメラ体を作製し、in vitroで検討を行った。ヒトCD26ではMERS-CoVのS蛋白結合領域の一部に相当するマウスCD26のaa326-340をヒト型に置換するだけで、MERS-CoVのマウス細胞に対する感染性を獲得できた。この結果から、ノックインする領域はaa326-340が最適である事が明らかになった。また、本年度はMERS-CoVの病理組織診断法を確立した。新生仔マウスにMERS-CoVを接種し、ウイルス分離ができた個体を陽性コントロールとし、*in situ* hybridization法に用いるプローブの検討とMERS-CoVのN蛋白に対する抗体の特異性を調べた。プローブでMERS-CoV遺伝子の検出は可能であった。また、免疫組織化学法により、MERS-CoVタンパクの検出も可能であった。さらに、この抗体はSARS-CoVとは交差せず、MERS-CoV特異的であった事から、SARS患者との鑑別が可能であると示された。今回確立した方法により、今後の臨床検体検査の対応が可能となった。

研究協力者：
岡村匡史（国立国際医療研究センター研究所感染症制御研究部）
永田典代（国立感染症研究所感染病理部）
鈴木忠樹（国立感染症研究所感染病理部）
中島典子（国立感染症研究所感染病理部）
佐藤由子（国立感染症研究所感染病理部）
福士秀悦（国立感染症研究所ウイルス第一部）
松山州徳（国立感染症研究所ウイルス第三部）
梁　明秀（横浜市立大学医学部）

A. 研究目的

中東呼吸器症候群コロナウイルス(MERS-CoV)は、2012 年に中東で発生が確認された新規のヒトコロナウイルスで、重症呼吸器症状と腎不全が主徴とされている。その症状から重症急性呼吸器症候群(SARS)との鑑別診断が必要で、現在まで (2015 年 2 月 5 日現在) に 965 人の確定患者がおり、そのうち 357 名が死亡している。流行は未だ続いており、今後の日本での流行に備えて診断、治療、防疫対策が急務である。そこで本研究では MERS-CoV に対し病原性の解明、ワクチンなどの有効性試験、ウイルス増殖部位の同定および免疫応答を詳細に検討するため、感染動物モデルの確立を試みる。さらに、これを利用して診断、治療および予防法の検討を行い、MERS-CoV の侵入に備える。本年度はヒト CD26 発現遺伝子改変マウスの作製を行った。また、MERS-CoV は臨床症状が SARS と類似しており、鑑別診断が必要である。そのため、MERS と SARS の鑑別が可能なパラフィン包埋組織切片を用いた病理組織診断法を確立した。

B. 研究方法

(1) ヒト CD26 発現マウス培養細胞における MERS-CoV 感染性の検討：

マウス線維芽細胞由来の NIH3T3 細胞に FugenHD を用いて、ヒト CD26 発現プラスミドをトランスフェクションした。トランスフェクション後、24 時間で 10^7 $TCID_{50}$/ml の MERS-CoV を MOI=0.1 のウイルス量で感染させた。感染後 0、1、2、3 日の上清を回収し、VeroE6 細胞における 50%細胞培養感染量($TCID_{50}$)を Kärver 法により算出し、感染性ウイルス量を測定した。

(2) ヒト CD26 発現遺伝子改変マウスの作製：

BDF1 マウス雌 20 匹に馬血清性性腺刺激ホルモンおよびヒト絨毛性性腺刺激ホルモンを投与し、過排卵処理を施した。その後、雄の C57BL/6 マウスと交配させ、前核期受精卵を得た。そして、環状のヒト CD26 遺伝子を含む細菌人工染色体(Bacterial Artificial Chromosome; BAC)を受精卵前核に注入し、注入後の受精卵を偽妊娠仮親 ICR マウスの卵管に移植した。得られた産仔の尾から DNA を抽出し、ヒト CD26 遺伝子の有無を PCR 法で確認した。

(3) ヒト CD26 とマウス CD26 cDNA キメラ体作製とそれらを発現させたマウス培養細胞での MERS-CoV 感染実験：

ヒト CD26 において、MERS-CoV の S タンパクが結合する領域にあたる cDNA

をマウス CD26 cDNA に置換したキメラ体を作製した。マウス CD26 の aa273-340 あるいはヒトとマウスでアミノ酸相同性が低い領域である aa273-290 または aa326-340 をヒト CD26 cDNA に置換したものをそれぞれ設計した(図 2A)。これらのキメラ体は PCR 法で作製し、発現プラスミドに組み込み、クローニングした。これらを NIH3T3 細胞に FugeneHD を用いてトランスフェクションし、24 時間後に 10^7 $TCID_{50}$/ml の MERS-CoV を MOI=0.1 のウイルス量で感染させた。感染後 0、1、2、3 日の上清を回収し、VeroE6 細胞における $TCID_{50}$ を Kärver 法により算出し、感染性ウイルス量を測定した。

(4) MERS-CoV の病理組織診断法に使用する MERS-CoV 陽性コントロールの作製:

MERS-CoV 10^7 $TCID_{50}$/ml を生後 24 時間以内の新生仔 ddY マウスに接種(10 μ l)した。接種後 14 日で解剖、組織を採材し、常法どおり 10%ホルマリン緩衝液固定後、パラフィン切片組織を作製し、病理学的解析を行った。また病変の見られた個体のパラフィン包埋組織から RNA を抽出し、MERS-CoV 遺伝子に対するリアルタイム RT-PCR を行い、感染を確認した。

(5) MERS-CoV に対する病理組織診断法の確立:

In situ hybridization 法によるウイルス遺伝子の検出には、MERS-CoV の E あるいは N 遺伝子を検出する二種類のプローブを混合して使用した。

免疫組織化学法によるウイルス抗原の検出は、MERS-CoV N タンパクに対するマウスモノクローナル抗体を用いて行った。

(倫理面への配慮)

動物実験は各研究機関および国立感染症研究所実験動物委員会の審査と承認を得て、動物愛護の精神に則り遂行した。また MERS-CoV を取り扱う実験は全て国立感染症研究所病原体等安全管理委員会規則に従って、使用および保管等を行った。遺伝子組換え実験は、遺伝子組換え生物等の使用(第二種使用)の承認を得た。

C. 結果

(1) ヒト CD26 発現マウス培養細胞における MERS-CoV 感染性の検討:

ヒト CD26 を発現させた NIH3T3 細胞に MERS-CoV を感染させると、感染 1 日目からウイルスの増殖が確認された(図 1)。感染量は VeroE6 細胞に MERS-CoV を感染させた場合より低かったが、ヒト CD26 が発現していない NIH3T3 細胞では、ウイルス増殖が全く見られなかったため、レセプターが発現していれば、マウス細胞で MERS-CoV は感染、増殖が可能であると確認された。

(2) ヒト CD26 発現遺伝子改変マウスの作製:

雌の BDF1 マウスから受精卵を回収し、ヒト CD26 遺伝子を含んだ BAC プラスミドを受精卵前核に挿入した後、それを 3 匹の仮親に子宮内移植した。移植後、15 匹の産仔が得られ、そのうち 10 匹でヒト CD26 遺伝子が PCR 法により確認できた。現在、これらの次世代マウスから産仔が得られたため、3-4 週齢に成長した後、ヒト CD26 の発現を確認し、感染実験を行う予定である。

(3) ヒト CD26 とマウス CD26 cDNA キメラ体作製とそれらを発現させたマウス培養細胞での MERS-CoV 感染実験：

作製したキメラ体を NIH3T3 細胞に発現させ、MERS-CoV を感染させると、aa273-340 をヒト型に置換したキメラ体はヒト CD26 を発現させた場合と同等の感染性および増殖性を獲得した (図 2B)。aa279-340 の領域でヒトとマウスのアミノ酸配列を比較した場合、相同性が低い aa273-290 または aa326-340 部位をそれぞれヒト型に置換したキメラ体の感染性は、aa273-290 置換型では、ほとんど感染性を示さなかったが、aa326-340 置換型はヒト CD26 を発現させた場合と同等のウイルス価を得た (図 2B)。この結果から、aa279-340 全域をヒト型にしなくても、aa326-340 の配列をマウスにノックインする事により、マウスは MERS-CoV に対してヒト CD26 を発現させた場合と同等の感染性を獲得できると考えられた。

(4) MERS-CoV の病理組織診断法に使用する MERS-CoV 陽性コントロールの作製:

生後 24 時間以内に MERS-CoV を接種した新生仔マウスは、感染 14 日後に 6 匹中 1 匹の割合で、ウイルス分離ができた。病変が確認できた個体のパラフィン包埋組織から RNA を抽出し、MERS-CoV のリアルタイム RT-PCR を行った。その結果、ウイルスゲノムが検出できたため、この個体は病理組織診断法の陽性コントロールに使用可能と考えられた。

(5) MERS-CoV に対する病理組織診断法の確立：

MERS-CoV の E あるいは N 遺伝子を検出する antisense および sense プローブを用いて、パラフィン包埋組織からウイルスゲノムが検出できた新生仔マウスの組織切片で *in situ* hybridization を行った。その結果、変性細胞の細胞質にウイルスゲノムおよび mRNA を検出する antisense プローブのシグナルが検出された。Sense プローブのシグナルは検出できなかった。この結果から、今回使用したプローブは MERS-CoV 遺伝子の検出が可能であると考えられた。

また、同じ個体の組織切片を用いて、MERS-CoV の N タンパクに対するマウスモノクローナル抗体で免疫組織化学法を行った。*In situ* hybridization と同様の細胞で抗原が検出された。さらに、この抗体を臨床症状が類似する SARS-CoV 感染患者の肺組織で免疫組織化学法を行ったところ、抗原は検出されず、SARS-CoV と交差しない事が明らかとなった。これらの結果を Table 1 にまとめた。

今回使用した陽性コントロールは SARS-CoV を検出するプローブや抗体には反応せず、MERS-CoV 検出の陽性コントロールとして適している事も明らかとなった。

D. 考察

ヒト CD26 発現遺伝子改変マウスは、次世代マウスのヒト CD26 タンパクの組織発現および局在を確認した後、感染実験に用いる予定である。ファウンダーマウスが 10 匹得られたが、ヒト CD26 を発現している系統が多かった場合は、発現量の異なる 2、3 系統を感染させ、MERS を発症する最適な系統を選択する。また、遺伝子改変マウスの第二世代として、ノックインマウスの開発に取り組むが、本年度に行った *in vitro* の基礎実験から、

aa326-340 をヒト型に置換するとマウス細胞で MERS-CoV の感染性を得られる事が分かったため、この部分をノックインしたマウスの作製を行う予定である。

本年度は MERS-CoV の病理組織診断法を確立できた。パラフィン包埋組織の陽性コントロールの作製、プローブの検討、抗体の特異性の検討が達成された。抗体に関しては SARS-CoV と鑑別可能であることも分かった。今後、臨床検体に対する検査依頼があった場合、対応が可能となった。その他の診断法と合わせて、MERS-CoV に対する有効な診断法と言える。

E. 結論

昨年度の研究で、マウスおよびラットは MERS-CoV の動物モデルに適さない事が明らかとなった。しかし、本年度にヒト CD26 発現遺伝子改変マウスが作製できたことにより、MERS-CoV 感染動物モデル確立の可能性は非常に高くなった。また次年度にノックインマウスが作製できれば、より理想的なモデルとなり得る。

そして、本年度はこれまで感染培養細胞でしか検討できなかった病理組織診断法を MERS-CoV 感染マウスの組織切片を陽性コントロールとする事により、パラフィン包埋組織切片での検討を可能にした。その結果、MERS-CoV の *in situ* hybridization 法や免疫組織化学法が確立でき、臨床検体の検査対応を可能とした。また免疫組織化学法については、SARS-CoV との鑑別診断に応用可能で、非常に有用な診断法である。

F. 健康危険情報

なし

G. 研究発表

1. 論文発表

1. Iwata-Yoshikawa N, Uda A, Suzuki T, Tsunetsugu-Yokota Y, Sato Y, Morikawa S, Tashiro M, Sata T, Hasegawa H, Nagata N. Effects of Toll-like Receptor Stimulation on Eosinophilic Infiltration in Lungs of BALB/c Mice Immunized with UV-inactivated Severe Acute Respiratory Syndrome-related Coronavirus Vaccine. J Virol. 2014 Aug;88(15):8597-614.

2. Nagata N, Saijo M, Kataoka M, Ami Y, Suzaki Y, Sato Y, Iwata-Yoshikawa N, Ogata M, Kurane I, Morikawa S, Sata T, Hasegawa H. Pathogenesis of fulminant monkeypox with bacterial sepsis after experimental infection with West African monkeypox virus in a cynomolgus monkey. Int J Clin Exp Pathol. 2014 Jun 15;7(7):4359-70.

3. Kotani O, Iwata-Yoshikawa N, Suzuki T, Sato Y, Nakajima N, Koike S, Iwasaki T, Sata T, Yamashita T, Minagawa H, Taguchi F, Hasegawa H, Shimizu H, Nagata N. Establishment of a panel of in-house polyclonal antibodies for the diagnosis of enterovirus infections. Neuropathology. 2014 Sep 28.

学会発表

1. 福士秀悦、永田典代、岩田奈織子、谷英樹、吉河智城、谷口怜、福間藍子、下島昌幸、西條政幸 高齢マウスにおける重症熱性血小板減少症候群ウイ

ルスの感染感受性の解析 第62回日本ウイルス学会(横浜)、2014年11月

2. 永田典代、岩田奈織子、鈴木忠樹、高橋健太、佐多徹太郎、長谷川秀樹、網康至、久保田耐、加藤篤、田代眞人、竹田誠、木所稔 動物モデルを用いたムンプスウイルスの神経病原性に関する病理学的検討 第62回日本ウイルス学会(横浜)、2014年11月

3. 小谷治、藤井健、鈴木忠樹、岩田奈織子、網康至、須崎百合子、長谷川秀樹、田口文広、清水博之、永田典代 カニクイザルを用いたSaffold virusの神経病原性の病理学的解析
第62回日本ウイルス学会(横浜)、2014年11月

4. 岩田奈織子、福士秀悦、福間藍子、鈴木忠樹、竹田誠、田代眞人、長谷川秀樹、永田典代 中東呼吸器症候群コロナウイルスに対するマウスおよびラットの感受性について 第62回日本ウイルス学会(横浜)、2014年11月

H. 知的財産の出願・登録状況

1. 特許取得
なし
2. 実用新案登録
なし
3. その他
なし

A

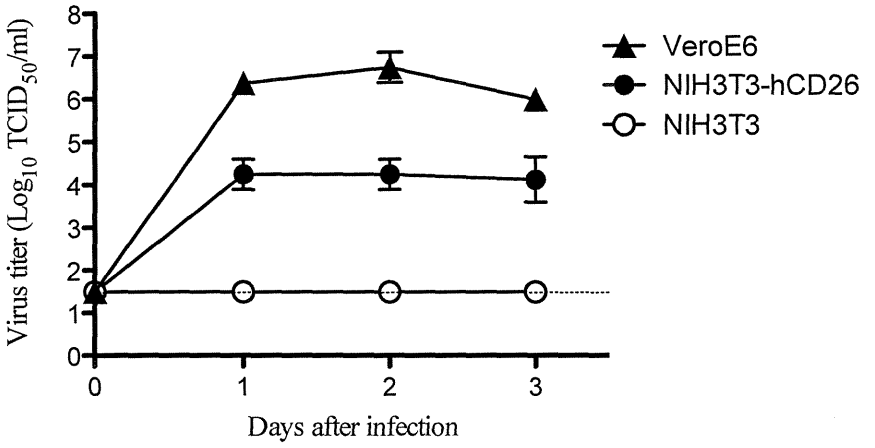

図 1　(A) VeroE6 細胞、ヒト CD26 発現 NIH3T3 細胞および NIH3T3 細胞の MERS-CoV 感染後 1, 2, 3 日に回収した上清のウイルス価。

A

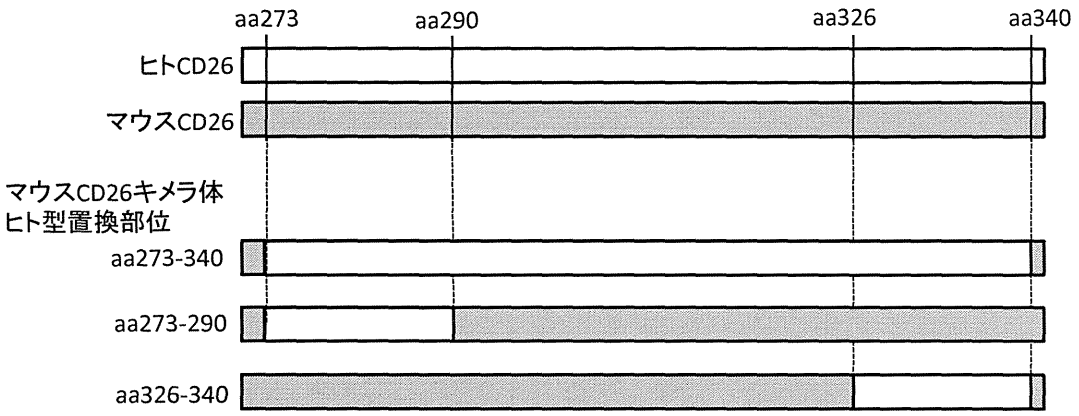

B

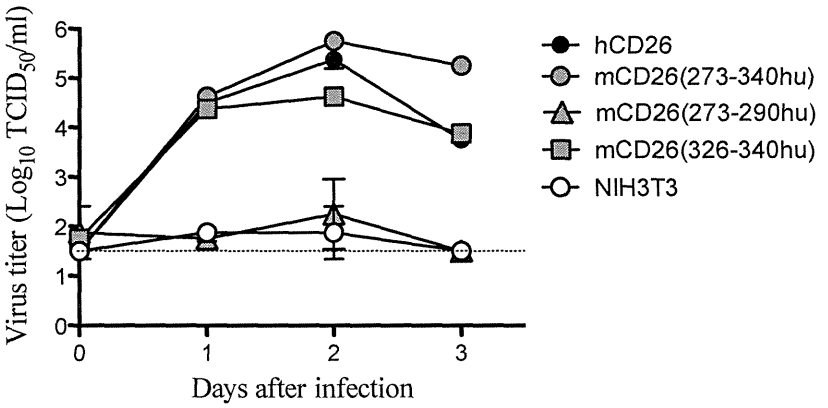

図 2　(A) マウス CD26 cDNA にヒト CD26 の MERS-CoV 結合部位を置換したキメラ体 3 種類。(B) マウス CD26 cDNA とヒト CD26 cDNA のキメラ体をトランスフェクションした NIH3T3 細胞に MERS-CoV を感染し、感染後 1, 2, 3 日の上清のウイルス価。ヒト CD26 cDNA をトランスフェクションしたものを陽性コントロールとした。

Table 1. MERS-CoV に対する病理学的診断法に用いた抗体およびプローブの特異性について

使用組織	MERS-CoV		SARS-CoV	
	Antibody	Probe	Antibody	Probe
MERS-CoV 感染マウス	+	+	-	-
SARS-CoV 感染患者	-	NA	NA (+)[1]	NA (+)[2]

[1] N. Nakajima *et al.*, JJID, 56, 139-141, 2003

[2] 中島典子 他 3 名、病理と臨床、vol.32 (no.10)、201

II. 研究成果の刊行に関する一覧表

研究成果の刊行に関する一覧表

発表者氏名	論文タイトル名	掲載誌名	巻号	ページ	出版年
Iwata-Yoshikawa N, Uda A, Suzuki T, Tsunetsugu-Yokota Y, Sato Y, Morikawa S, Tashiro M, Sata T, Hasegawa H, Nagata N.	Effects of Toll-like Receptor Stimulation on Eosinophilic Infiltration in Lungs of BALB/c Mice Immunized with UV-inactivated Severe Acute Respiratory Syndrome-related Coronavirus Vaccine.	Journal of Virology	88	8597-614	2014

III. 研究成果の刊行物・別刷

JVI
Journals.ASM.org

Effects of Toll-Like Receptor Stimulation on Eosinophilic Infiltration in Lungs of BALB/c Mice Immunized with UV-Inactivated Severe Acute Respiratory Syndrome-Related Coronavirus Vaccine

Naoko Iwata-Yoshikawa,[a] Akihiko Uda,[b] Tadaki Suzuki,[a] Yasuko Tsunetsugu-Yokota,[c]* Yuko Sato,[a] Shigeru Morikawa,[b] Masato Tashiro,[d] Tetsutaro Sata,[a] Hideki Hasegawa,[a] Noriyo Nagata[a]

Department of Pathology,[a] Department of Veterinary Science,[b] Department of Immunology,[c] and Influenza Virus Research Center,[d] National Institute of Infectious Diseases, Tokyo, Japan

ABSTRACT

Severe acute respiratory syndrome-related coronavirus (SARS-CoV) is an emerging pathogen that causes severe respiratory illness. Whole UV-inactivated SARS-CoV (UV-V), bearing multiple epitopes and proteins, is a candidate vaccine against this virus. However, whole inactivated SARS vaccine that includes nucleocapsid protein is reported to induce eosinophilic infiltration in mouse lungs after challenge with live SARS-CoV. In this study, an ability of Toll-like receptor (TLR) agonists to reduce the side effects of UV-V vaccination in a 6-month-old adult BALB/c mouse model was investigated, using the mouse-passaged Frankfurt 1 isolate of SARS-CoV. Immunization of adult mice with UV-V, with or without alum, resulted in partial protection from lethal doses of SARS-CoV challenge, but extensive eosinophil infiltration in the lungs was observed. In contrast, TLR agonists added to UV-V vaccine, including lipopolysaccharide, poly(U), and poly(I·C) (UV-V+TLR), strikingly reduced excess eosinophilic infiltration in the lungs and induced lower levels of interleukin-4 and -13 and eotaxin in the lungs than UV-V-immunization alone. Additionally, microarray analysis showed that genes associated with chemotaxis, eosinophil migration, eosinophilia, and cell movement and the polarization of Th2 cells were upregulated in UV-V-immunized but not in UV-V+TLR-immunized mice. In particular, CD11b$^+$ cells in the lungs of UV-V-immunized mice showed the upregulation of genes associated with the induction of eosinophils after challenge. These findings suggest that vaccine-induced eosinophil immunopathology in the lungs upon SARS-CoV infection could be avoided by the TLR agonist adjuvants.

IMPORTANCE

Inactivated whole severe acute respiratory syndrome-related coronavirus (SARS-CoV) vaccines induce neutralizing antibodies in mouse models; however, they also cause increased eosinophilic immunopathology in the lungs upon SARS-CoV challenge. In this study, the ability of adjuvant Toll-like receptor (TLR) agonists to reduce the side effects of UV-inactivated SARS-CoV vaccination in a BALB/c mouse model was tested, using the mouse-passaged Frankfurt 1 isolate of SARS-CoV. We found that TLR stimulation reduced the high level of eosinophilic infiltration that occurred in the lungs of mice immunized with UV-inactivated SARS-CoV. Microarray analysis revealed that genes associated with chemotaxis, eosinophil migration, eosinophilia, and cell movement and the polarization of Th2 cells were upregulated in UV-inactivated SARS-CoV-immunized mice. This study may be helpful for elucidating the pathogenesis underlying eosinophilic infiltration resulting from immunization with inactivated vaccine.

Severe acute respiratory syndrome-related coronavirus (SARS-CoV), a cause of severe respiratory illness, emerged in southern China in late 2002 and quickly spread to several countries throughout Asia, Europe, and North America by early 2003 (1–4). Although SARS has not reemerged since 2003, vaccination is the most likely mode of preventing future SARS-CoV outbreaks, especially in individuals at high risk, such as health care workers. To date, no vaccine is licensed for SARS-CoV. A SARS-CoV vaccine based on whole inactivated virions is easily prepared and is expected to induce a broader spectrum of antibodies than recombinant virus-based vaccines expressing particular sets of SARS-CoV proteins. Although inactivated whole SARS-CoV vaccines induce neutralizing antibodies in mouse models (5–10), they also cause increased eosinophilic immunopathology in the lungs upon SARS-CoV challenge (11–14). These reactions are thought to be caused by the incorporation of SARS-CoV nucleocapsid protein (N) in vaccine formulations, which induces N-specific immune responses and enhances eosinophilic immune pathology (11, 12, 15).

Enhanced eosinophilic immune pathology was also observed in the 1960s, when formalin-inactivated respiratory syncytial virus (FI-RSV) vaccine combined with alum adjuvant was injected intramuscularly into children to immunize them against RSV. In these trials, 80% of immunized children were hospitalized and died of enhanced respiratory disease upon subsequent RSV infec-

Received 8 April 2014 Accepted 13 May 2014
Published ahead of print 21 May 2014
Editor: S. Perlman
Address correspondence to Noriyo Nagata, nnagata@niid.go.jp.
* Present address: Yasuko Tsunetsugu-Yokota, Tokyo University of Technology, Tokyo, Japan.
Supplemental material for this article may be found at http://dx.doi.org/10.1128/JVI.00983-14.

doi:10.1128/JVI.00983-14

tion. Histologic examination of their lungs showed bronchoconstriction and severe pneumonia with peribronchiolar eosinophils (16, 17). These findings suggest that FI-RSV vaccination induced nonneutralizing, nonprotective antibodies, with natural infection of RSV causing a hypersensitivity response to viral antigens, characterized by bronchoconstriction and severe pneumonia. The pathology of the enhanced respiratory disease upon subsequent RSV infection is thought to be due to skewing of the immune response toward Th2, with eosinophils having a key role in the progression of enhanced respiratory disease. The generation of nonprotective antibodies by the FI-RSV vaccine may have been due to poor Toll-like receptor (TLR) stimulation (18).

Thus, TLR stimulation with an inactivated whole virion vaccine is thought to be crucial to induce protective antibodies and to reduce eosinophilic responses. In this study, we evaluated the efficacy and safety of UV-inactivated whole SARS-CoV (UV-V) in a model using BALB/c mice and mouse-passaged SARS-CoV. We investigated the ability of adjuvant TLR agonists to reduce the side effects of UV-V vaccination, such as enhanced eosinophilic immune pathology.

MATERIALS AND METHODS

Viruses and cells. Vero E6 cells, purchased from the American Type Culture Collection (Manassas, VA), were cultured in Eagle's minimal essential medium (MEM) containing 5% fetal bovine serum (FBS), 50 IU/ml penicillin G, and 50 μg/ml streptomycin. Stocks of the mouse-passaged Frankfurt 1 isolate of SARS-CoV, F-musX-VeroE6 (F-musX), were propagated and titrated on Vero E6 cells and cryopreserved at −80°C as previously described (19). Viral infectivity titers are expressed as 50% of the tissue culture infectious dose ($TCID_{50}$)/ml on Vero E6 cells, as calculated according to the Behrens-Kärber method. Work with infectious SARS-CoV was performed under biosafety level 3 conditions.

Preparation of UV-V. UV-V was prepared as previously described (6). Briefly, the HKU39849 isolate of SARS-CoV was amplified in Vero E6 cells, exposed to UV light (4.75 J/cm^2), and purified by sucrose density gradient centrifugation. Inactivation of the virus infectivity of UV-V was confirmed upon inoculation into Vero E6 cells.

Animal experiments. BALB/c female mice, purchased from Japan SLC Inc. (Shizuoka, Japan), were housed in an environmentally controlled specific-pathogen-free animal facility. Animals were infected with SARS-CoV in biosafety level 3 animal facilities, according to the Animal Care and Use Committee of the National Institute of Infectious Diseases, Tokyo, Japan.

For immunization, 14-week-old BALB/c mice were subcutaneously injected in the back with 10 μg UV-V alone (UV-V), 10 μg UV-V plus 2 mg alum (Pierce, Rockford, IL) (UV-V+Alum), or 10 μg UV-V plus TLR agonists (UV-V+TLR) and reimmunized 6 to 7 weeks later. The TLR agonists consisted of 1 μg lipopolysaccharide (LPS) (Sigma-Aldrich, St. Louis, MO), 2.5 μg poly(I·C) (Invitrogen, San Diego, CA), and 0.1 μg poly(U) (Invitrogen) per immunization. Control mice were injected with phosphate-buffered saline (PBS) with or without alum.

At 8 to 10 days after the 2nd immunization, mice were anesthetized by intraperitoneal injection of a mixture of 1.0 mg ketamine and 0.02 mg xylazine in 0.1 ml/10 g body weight. The animals were subsequently inoculated in the left nostril with $10^{6.5}$ $TCID_{50}$ of F-musX in 30 μl, 1,000-fold higher than the 50% lethal dose for adult BALB/c mice (n = 5 to 7 per group) (19).

A second vaccination experiment was performed to evaluate the long-term efficacy of TLR, with the vaccinated mice rested for 4 weeks before F-musX challenge. Ten-week-old BALB/c mice were vaccinated with 10 μg UV-V or 10 μg UV-V+TLR and boosted 6 weeks later. Four weeks afterwards, the animals were inoculated in the left nostril with $10^{6.5}$ $TCID_{50}$ in 30 μl of F-musX.

To mimic immunization with an attenuated vaccine, 25-week-old mice were administered $10^{6.3}$ $TCID_{50}$ of the HKU39849 isolate in 20 μl intranasally, since HKU39849 was shown to be avirulent in adult mice. Control mice were injected with MEM intranasally. Fourteen days later, these mice were challenged intranasally with $10^{6.5}$ $TCID_{50}$ in 30 μl of F-musX.

Body weights were measured daily for 10 days, and the mice were sacrificed 3 or 10 days after challenge to analyze virus replication, hematology, cytokine expression, and pathology (n = 3 to 4 per group).

Virus titration. To titrate virus infectivity in lung homogenates, 10% (wt/vol) tissue homogenates of each lung were prepared in MEM containing 2% FBS, 50 IU/ml penicillin G, 50 μg/ml streptomycin, and 2.5 μg/ml amphotericin B. Lung wash fluid was also collected for analysis of infectious virus titers.

Cytokine and chemokine profiling. Inflammatory profiling of 10% (wt/vol) lung homogenates was performed using the Milliplex Map assay (Millipore, MA), as described by the manufacturer. These assays can determine the concentrations of 18 cytokines and chemokines, including eotaxin, granulocyte-macrophage colony-stimulating factor (GM-CSF), gamma interferon (IFN-γ), interleukin 1β (IL-1β), IL-2, IL-4, IL-5, IL-6, IL-7, IL-10, IL-12 (p70), IL-13, gamma interferon-induced protein 10 (IP-10), neutrophil-related chemokine KC (KC), monocyte chemoattractant protein 1 (MCP-1), macrophage inflammatory protein 1α (MIP-1α), regulated and normal T cell expressed and secreted (RANTES), and tumor necrosis factor alpha (TNF-α). Type I IFNs in 10% (wt/vol) lung homogenates obtained 3 and 10 days after inoculation were analyzed using mouse alpha and beta IFN (IFN-α and -β) enzyme-linked immunosorbent assay (ELISA) kits (PBL Interferon Source, Piscataway, NJ), according to the protocol described by the manufacturer.

SARS-CoV neutralizing assay. Blood was obtained from the tail vein of each mouse and allowed to clot. Sera were collected by centrifugation and inactivated by incubation at 56°C for 30 min. One hundred $TCID_{50}$ aliquots of F-musX of SARS-CoV were incubated for 1 h in the presence or absence of mice sera serially 2-fold diluted and then added to confluent Vero E6 cell cultures in 96-well microtiter plates as described previously (20). The presence of a viral cytopathic effect was determined on day 3, and the titers of neutralizing antibody were determined as the reciprocal of the highest dilution at which cytopathic effect was not observed. The lowest and highest serum dilutions tested were 1:2 and 1:512, respectively.

Quantitative real-time reverse transcription (RT)-PCR. To assay type I IFN mRNA expression and viral genome copies during early phases of SARS-CoV infection, the left lobe of a lung from mice injected with UV-V (n = 6), UV-V+TLR (n = 6), or PBS (n = 3) was obtained 1 day after challenge and placed in RNAlater solution (Ambion). RNA was extracted from the lung samples using RNeasy minikits (Qiagen, Hilden, Germany), according to the manufacturer's instructions.

Real-time one-step quantitative RT-PCR assays were used to detect IFN-α4, IFN-β, and SARS-CoV mRNA using QuantiTect Probe RT-PCR kits (Qiagen, Valencia, CA) and an ABI Prism 7900HT Fast real-time PCR system (Applied Biosystems, Foster City, CA). TaqMan probes and primers are listed in Table 1. Reaction mixtures were incubated at 50°C for 30 min, followed by 95°C for 15 min and thermal cycling, which consisted of 40 cycles of denaturation at 94°C for 15 s, and annealing and extension at 60°C for 60 s. The expression of each gene was normalized relative to that of β-actin mRNA, with the expression of IFN-α4 and IFN-β mRNAs calculated as the $\log_{10}$ fold change relative to results with PBS-injected and challenged mice.

Histopathology and immunohistochemistry. Animals were anesthetized and perfused with 2 ml of 10% phosphate-buffered formalin (n = 3 to 4). Animals were necropsied within 12 h of death, whereas moribund animals were euthanized by excess isoflurane. All animals were subsequently examined histopathologically, with 10% phosphate-buffered formalin injected into the trachea until the lungs inflated. Fixed lung tissues were routinely embedded in paraffin, sectioned, and stained with hematoxylin and eosin. Eosinophils were identified with a C.E.M. kit using

TABLE 1 Primers and probes for quantitative real-time RT-PCR

Target (reference)	Sequence
IFN-α4	
Forward	CAACTCTACTAGACTCATTCTGCAAT
Reverse	AGAGGAGGTTCCTGCATCACA
Probe	ACCTCCATCAGCAGCTCAATGACCTCAAA
IFN-β	
Forward	GCTCCTGGAGCAGCTGAATG
Reverse	TCCGTCATCTCCATAGGGATCT
Probe	TCAACCTCACCTACAGGGCGGACTTC
SARS-CoV N gene (56)	
Forward	AGGAACTGGCCCAGAAGCTT
Reverse	AACCCATACGATGCCTTCTTTG
Probe	ACTTCCCTACGGCGCTA
β-Actin	
Forward	ACGGCCAGGTCATCACTATTG
Reverse	CAAGAAGGAAGGCTGGAAAAGA
Probe	CAACGAGCGGTTCCGATGCCC

Astra Blue/Vital New Red staining (DBS, Pleasanton, CA). For Astra Blue/Vital New Red-stained slides, five 240-μm^2 sections in the extrabronchioles were assessed, and the eosinophils, neutrophils, lymphocytes, and macrophages counted were averaged per lung of each mouse. Immunohistochemical detection of SARS-CoV antigens was performed on paraffin-embedded sections, as previously described (19).

Isolation of CD11b-positive ($CD11b^+$) lung cells. Whole lungs were collected from mice 1 day after challenge with F-musX, and their $CD11b^+$ cells were isolated by a modification of previous protocols (21). Briefly, mice were euthanized under excess anesthesia, and the lungs were perfused via the left ventricle with 20 ml of PBS containing 10 U/ml of heparin (Novo Nordisk Pharma Ltd., Novo Alle, Denmark) to remove red blood cells (RBCs). The lungs were removed aseptically, cut into 1-mm pieces, and incubated in HEPES buffer containing collagenase D (2 mg/ml; Roche Applied Science, Mannheim, Germany) and bovine pancreatic DNase I (40 U/ml; Sigma-Aldrich) for 30 to 45 min at 37°C. Single-cell suspensions were prepared by gently pushing the tissue through a 70-μm nylon screen, followed by washing and centrifugation at 2,000 rpm. To isolate $CD11b^+$ cells, the single-cell suspensions were washed with PBS containing 0.5% FBS (PBS-FBS), counted, and incubated at the appropriate ratio with MACS CD11b microbeads (Miltenyi Biotec, Auburn, CA) for 15 min at 4°C. After washing again with 10 ml of PBS-FBS, the cells were diluted in 3 ml of PBS-FBS. Finally, the $CD11b^+$ cells were separated by passing the antibody-coated cell suspension over an MS-positive selection column on a SuperMACS magnetic cell separator (Milteni Biotec). $CD11b^+$ cells were collected by removing the column from the magnetic field and then flushing it with PBS-FBS. Purity was checked by flow cytometry. To confirm the morphology of the obtained cells, around 1×10^5 cells in 100 μl of PBS-FBS were centrifuged at 1,000 rpm for 10 min onto glass slides using a Shandon cytocentrifuge (Thermo Fisher Scientific Inc., Waltham, MA). These cells were stained with Giemsa stain and analyzed by microscopy.

Flow cytometry analysis. The lung $CD11b^+$ cells were washed with PBS-FBS. After blocking Fc receptors by incubating 1 μg of anti-mouse CD16/CD32 monoclonal antibody (MAb) (BD Pharmingen, San Jose, CA) per 10^6 cells for 20 min on ice, the cells were stained for 30 min on ice with allophycocyanin (APC)-conjugated anti-mouse CD11b (BioLegend Inc., San Diego, CA). The cells were washed twice in PBS-FBS and fixed with 2% paraformaldehyde. Flow cytometry was performed on a FACSCanto II instrument (Becton, Dickinson, San Diego, CA), with the data analyzed using the FlowJo 8.7.1 software program (Treestar, Ashland, OR).

Microarray analysis. Microarray analysis was performed using left lung lobe tissue samples and $CD11b^+$ cells in the lung, as described previously (22). Briefly, total RNA was extracted using an RNeasy minikit (Qiagen, Hilden, Germany), according to the manufacturer's instructions. RNA concentrations were measured with an ND-1000 spectrophotometer (Nanodrop Technologies, Wilmington, DE). The quality of the RNA samples was assessed spectroscopically, and the quality of the intact RNA was assessed using an Agilent 2100 bioanalyzer (Agilent Technologies, Inc., Palo Alto, CA). RNA samples with the highest RNA integrity number, of more than 7, as determined by the bioanalyzer, were used for microarray analysis. Two hundred micrograms (lung tissue) or 25 μg ($CD11b^+$ cells) of total RNAs was used for amplification and labeled using a low-RNA-input linear amplification kit (Agilent).

Individual cRNA samples were fragmented by incubation with fragmentation buffer and blocking agent at 60°C for 30 min (gene expression hybridization kit [Agilent]). These RNA samples were hybridized at 65°C for 17 h at 10 rounds per min to a SurePrint G3 Mouse GE 8 by 60,000 microarray (Agilent). Controls consisted of RNA samples from mice injected with PBS, applied in duplicate to the slides; single samples were applied for all other RNA samples. The microarray slides were washed with wash solutions 1 and 2 (Agilent) and acetonitrile (Wako, Osaka, Japan). The slides were scanned with a DNA microarray scanner (Agilent), the images were analyzed using the Feature Extraction software program (Agilent), and the data files were automatically exported. Data mining was performed using the GeneSpring GX 12.1 software program (Agilent). Briefly, the text file exported by Feature Extraction software was imported into GeneSpring. The raw data were normalized per chip to the 75th percentile expression level and per gene to the median expression intensity of all samples. The samples of lung tissue were classified into four groups based on the treatment regimen: six mice each were immunized with UV-V, UV-V+TLR, and HKU39849, and three mice each were injected with PBS, yielding a total of six microarrays because the PBS samples were run in duplicate. $CD11b^+$ cell samples were classified into four groups based on the treatment regimen: six mice each were infected with F-musX and immunized with UV-V or UV-V+TLR, and six mice each were mock infected and immunized with UV-V or UV-V+TLR. Since the differences in individual gene expression within each group were small, all data are presented as the mean per group. Significant differences in gene expression between the UV-V and UV-V+TLR groups was assessed using one-way analysis of variance (ANOVA), followed by Tukey's honestly significant difference *post hoc* test and the Benjamini-Hochberg correction test, with P values of ≤ 0.05 considered statistically significant, and further filtered by $\geq$2-fold expression. Genes that met these criteria were characterized using Ingenuity Pathway Analysis (IPA) (Ingenuity Systems, Redwood City, CA) function annotations. All microarray slide hybridizations were performed using mouse oligonucleotide arrays (G4852A; Agilent).

Statistical analysis. Intergroup comparisons were performed by one-way ANOVA followed by Turkey's *post hoc* test using the GraphPad Prism 5 software program (GraphPad Software Inc., CA). P values less than 0.05 were considered statistically significant.

Microarray data accession numbers. The microarray results obtained in this work have been deposited in the Gene Expression Omnibus (GEO) (http://www.ncbi.nlm.nih.gov/projects/geo/) and assigned accession numbers GSE44274 (lung tissue) and GSE50855 ($CD11b^+$ cells isolated from lung).

RESULTS

Immunization with UV-V induces eosinophilic infiltrations in the lungs of adult mice after SARS-CoV challenge. To confirm an induction of eosinophilic immunopathology by immunization with UV-V in the adult mouse model (19), 11 mice per group were immunized with the vaccine and challenged 10 days after boosting with the live virus. All of the control mice, injected with PBS and alum (PBS+Alum), died of acute respiratory illness within 5 days

after infection with the live virus (Fig. 1A). In contrast, UV-V+Alum-immunized mice showed mild illness, such as hunching, ruffled fur, and body weight loss, within 3 days of infection and then recovered by day 5 (Fig. 1A). UV-V-immunized mice showed various levels of body weight loss and respiratory illness upon virus challenge. One mouse immunized with UV-V and one immunized with UV-V+Alum died on day 5. Virus titers in the lungs on day 3 did not differ significantly among UV-V-immunized, UV-V+Alum-immunized, and PBS+Alum-injected mice ($n = 3$ each) (Fig. 1B). In contrast, titers of virus in lung wash fluid on day 3 were significantly lower in UV-V+Alum-immunized mice than in PBS+Alum-injected mice. On the day before challenge with live virus, the serum titers of neutralizing antibodies were significantly higher in UV-V+Alum- than in UV-V-immunized mice ($n = 11$ each) (Fig. 1C) but did not differ significantly after challenge. The PBS+Alum-injected mice did not show seroconversion against SARS-CoV after challenge. Microscopic analysis of the lung sections of mice at 3 days after infection showed a high level of eosinophil infiltration around the bronchi in UV-V- and UV-V+Alum-immunized mice (Fig. 1D), whereas lymphocytes, macrophages, and a few neutrophils had infiltrated into the lungs of PBS+Alum-injected mice (Fig. 1D). Eosinophil infiltration was more severe on day 10 than on day 3 in UV-V- and UV-V+Alum-immunized mice. Histopathologically, both UV-V- and UV-V+Alum-immunized mice showed infiltration of inflammatory cells, including eosinophils, surrounding the bronchi and blood vessels on day 3 ($n = 3$ each) (Fig. 1E), consistent with previous results (13). We also investigated the lung pathology of the mice that died by day 5. Surprisingly, the lungs of both the UV-V- and UV-V+Alum-immunized mice showed high eosinophilic infiltration into areas surrounding the bronchi and blood vessels and severe inflammatory infiltrations in the alveoli (Fig. 2). Immunohistochemical analysis showed that a few SARS-CoV antigen-positive cells were present in the bronchiolar epithelial cells and alveolar cells of the dead UV-V-immunized mouse but were not present in cells of the dead UV-V+Alum-immunized mouse (Fig. 2). Although the virus neutralization titers in the sera on the day prior to virus challenge were 1:4 and 1:128 in the UV-V- and UV-V+Alum-immunized mice, respectively, these mice were unable to survive following SARS-CoV infection. In contrast, PBS+Alum-injected mice showed severe pulmonary edema, congestion, and hemorrhage, with many viral antigen-positive cells in the alveoli 5 days after challenge. We assumed that the severe respiratory illness in the dead UV-V- and UV-V+Alum-immunized mice was caused by an exacerbation of pulmonary inflammatory reactions due to UV-V acting as an inactivated RSV vaccine (18). The excess pulmonary eosinophilic infiltration possibly resulted from host immune responses rather than from a direct cytopathic effect caused by SARS-CoV replication.

Considering the excess eosinophilic immunopathology following SARS-CoV infection in mice immunized with inactivated virus, we examined whether the natural course of immune response elicited after nonlethal SARS-CoV infection resulted in excess eosinophil infiltration in the lungs of the reinfected mice. Mice were infected with the HKU39849 isolate, which induces nonlethal infection of both young and adult BALB/c mice, and challenged with F-musX. None of the HKU39849-inoculated mice showed clinical illness, as assessed by the absence of ruffled fur, dyspnea, and weight loss, and all survived after F-musX challenge (Fig. 3A). Titers of virus in the lungs of control mice were high on day 3 (10^8 $TCID_{50}$/g), although titers in the lungs and lung wash fluids of HKU39849-inoculated mice on days 3 and 10 after challenge were below the limit of detection (Fig. 3B). Virus neutralization titers in the sera on the day prior to virus challenge were higher than 1:16 (Fig. 3C). Histopathologically, the lungs of HKU39849-inoculated mice showed mild perivascular and peribronchiolar mononuclear cell infiltration on days 3 and 10 after the challenge (Fig. 3D and E). Most of these infiltrating cells were lymphocytes, with no eosinophils, and there were no cells positive for viral antigens in the lungs. In contrast, MEM-treated control mice showed severe respiratory illness and weight loss after F-musX infection and succumbed to infection within 5 days (Fig. 3A). The lung pathology of these control mice was similar to that of PBS+Alum-injected mice following challenge with SARS-CoV (data not shown). Thus, inoculation with HKU39849, mimicking immunization with attenuated live vaccine, provided a high level of protective immunity against SARS-CoV infection and elicited mild lymphocytic but not eosinophil infiltration in the lung after reinfection with F-musX.

Immunization with UV-V plus TLR agonists inhibits skewing to a Th2 response and high eosinophilic infiltration into the lungs of adult mice after challenge infection. We hypothesized that the excess pulmonary eosinophilic infiltration observed in mice immunized with UV-V was due to poor Toll-like receptor (TLR) stimulation as shown in FI-RSV vaccination (18). TLR agonists were used to induce host immune responses, especially innate immune responses, to virus infection (23, 24). Recognition by TLRs induces innate immune responses and eventually leads to activation of antigen-specific immunity (23). In addition, inactivated RSV vaccine-induced pulmonary disease was resolved by the addition of TLR agonists in an RSV mouse model (18). Therefore, we investigated the effect of TLR agonists as an adjuvant during immunization with UV-V. Within 3 days of challenge infection, UV-V+TLR-immunized mice developed a clinical illness, characterized by weight loss, hunching, and ruffled fur, but recovered by day 4 (Fig. 4A). By day 10, the body weight of all mice had recovered to that before immunization, and no mice had died (Fig. 4B). The survival rates, weight loss, and clinical illness of UV-V- and UV-V+TLR-immunized mice did not differ significantly. Viral titers in lung wash fluid but not in the lungs were significantly lower in UV-V+TLR-immunized mice than in PBS-injected mice on day 3 postinfection (p.i.) (Fig. 4C). Both UV-V- and UV-V+TLR-immunized mice showed seroconversion against SARS-CoV after the booster injection, with the titers of neutralizing antibodies on day 10 tending to be higher in UV-V+TLR-immunized than in UV-V-immunized mice (Fig. 4D). Interestingly, slight eosinophilic infiltration was observed in the lungs of UV-V+TLR-immunized mice on day 3 but not on day 10 (Fig. 4E). On day 10, lymphocytes were the primary infiltrating cells around vessels in the lungs of these mice. The numbers of eosinophils in the lungs were significantly lower in UV-V+TLR-immunized than in UV-V-immunized mice (Fig. 4F). Cytokine and chemokine responses were assessed in lung homogenates of UV-V- and UV-V+TLR-immunized mice on days 3 and 10. The levels of the Th2-related inflammatory cytokines IL-4 and IL-13 and the eosinophil-related chemokine eotaxin (CCL11) were lower in UV-V+TLR- than in UV-V-immunized mice on days 3 and 10 (Fig. 5). In contrast, the levels of IP-10 (CXCL10) and KC (CXCL1) tended to be higher in UV-V+TLR- than in UV-V-immunized mice on day 3. There were no significant